Formulation of stress concentration factors for concrete-filled steel tubular (CFST) T-joints under axial force in the brace

Jian Zheng [1], Shozo Nakamura [1,*], Yajing Ge [1], Kangming Chen [2], Qingxiong Wu [2]

[1] Dept. of Civil and Environmental Eng., Nagasaki University, 1-14, Bunkyo-machi, Nagasaki 852-8521, Japan

[2] College of Civil Eng., Fuzhou University, No. 2, Xueyuan Road, Fuzhou 350116, China

[*]Corresponding author：Shozo Nakamura

Tel: +81 95-819-2613

E-mail address: shozo@nagasaki-u.ac.jp

First author: Jian Zheng

E-mail address: zhengjianfzu@163.com

Third author: Yajing Ge

Email address: bb52116503@ms.nagasaki-u.ac.jp

Forth author: Kangming Chen

E-mail address: chen-kang-ming@163.com

Fifth author: Qingxiong Wu

E-mail address: wuqingx@fzu.edu.cn

Abstract

CFST T-joints consisting of a concrete-filled circular chord and a circular hollow section brace have been used in CFST trussed arch bridges. The stress concentration factors (SCFs) of CFST T-joints have been found to be much lower than those of circular hollow section (CHS) T-joints in the existing researches. At present, no parametric formulae have been proposed for SCFs determination for fatigue design of CFST T-joints. In this study, three-dimensional finite element (FE) models of the existing experiments for CFST T-joints were developed to determine the SCFs distribution at the chord-brace intersection under axial force in the brace. After confirming the validity of the FE models by the comparison of calculated SCFs with existing experimental results, they were provided for the parametric analysis to reveal the influence of four non-dimensional parameters, i.e. diameter ratio (β), diameter to thickness ratio of chord (2γ), thickness ratio (τ) and relative chord length (α), on SCFs of CFST T-joints. In total, 212 FE models with different parameters were analyzed under tensile and compressive axial forces. Based on the results of parametric analysis, a series of parametric formulae to calculate the SCFs was proposed for CFST T-joints referring to those for CHS T-joints. The SCFs determined by the formulae showed good agreements with FE analysis results.

Key words: CFST T-joints; Stress concentration factors; Hot spot stress; Fatigue; Finite element analysis; Parametric formulae.

1 Introduction

After the construction of the first CFST arch bridge, Wangcang East River Bridge in 1990, CFST trussed arch bridges have become very popular, and more than 400 CFST arch bridges have been constructed in the last 25 years in China. Their arch ribs can be categorized into solid type and trussed type, and the latter accounts for about 38% [1]. The trussed arch ribs consist of concrete-filled circular chords and circular hollow braces generally connected with full penetration butt welds to form CFST joint, including T-joints, Y-joints, K-joints, N-joints and so on. The filled-in concrete delays bucking of steel tube, and improves its compressive strength and ductility. However, the intersection with full penetration butt welds in CFST joint can be the weak part in the whole structure since the axial stiffness of brace is much larger than the radial stiffness of chord tube, which leads to high stress concentration around the chord-brace intersection. In fact, the fatigue cracks seriously damaging the structural safety were found in the chord-brace intersection of a half-through CFST trussed arch bridge in China [2].

Fatigue life of tubular joints is commonly related to the SCFs at the weld toes of the chord-brace intersection. So far, many studies to formulate the SCFs of various types of CHS joints as functions of main structural parameters have been carried out by many researchers, such as Kuang et al. [3], Efthymiou and Durkin [4], Hellier et al. [5], Smedley and Fisher [6], Mashiri et al. [7] and Zhao et al. [8]. The developed SCF formulae for the chord-brace intersection have been extensively adopted in many current national and international design codes for fatigue evaluation of the joints by hot spot stress (HSS) method [9-13]. However, there has not been many studies on fatigue of CFST joints to date and the appropriate SCFs formulae for them are rarely found in literatures and design codes. In addition, the Chinese code (JTG/T D65-06-2015) only gives allowable value of nominal stress amplitude for the fatigue checking calculation of CFST joints [14].

Tong et al. [15] experimentally investigated the SCFs of CFST K-joints, and revealed that they have more uniform distribution and obviously smaller values than CHS K-joints. Mashiri [16] found that the SCFs of CFST T-joint are generally lower than those of CHS T-joint under in-plane bending in the brace. By means of static test for CFST T-joints, Wang [17, 19], Chen [18, 20] and Xu [21] determined the SCFs and compared them with those estimated by some existing formulae for CHS T-joints.

Very limited studies have been conducted on the SCF formulae of CFST T-joints. Wang [19] and Chen [20] considered that filled-concrete can improves the local stiffness at the chord-brace intersection of CFST T-joints and its effect can be equivalent to the increase of chord wall thickness. They proposed a determination method of the equivalent chord wall thickness to use the existing SCF formulae for CHS T-joints. However, the SCFs calculated by the method were generally larger than the experimental investigation, especially under axial compressive force in the brace. In addition, the validity range of diameter to thickness ratio of chord 2γ in the method does not much its practical range of bridge structures. Furthermore, the influence of relative chord length α on SCFs is not investigated.

In this study, FE models to evaluate the SCFs of CFST T-joint (see **Fig. 1**) were developed first. After validating them by the comparison with existing experimental results in [18, 20, 21], they were provided for parametric analysis. Then, based on the parametric analysis results, SCF formulae of CFST T-joints subjected to axial force in the brace were proposed as functions of key non-dimensional geometric parameters. Finally, the accuracy of the formulae was verified by comparing the SCFs obtained by the formulae and FE analysis.

2 Validation of FE modelling

2.1 Brief summary of experimental studies on SCFs of CFST T-joints

The experiments to determine SCFs for CFST T-joints with different geometric parameters were carried out and published in [17, 18, 20, 21]. The loading methods are shown in **Fig. 2**. One end of chord was fixed, and another end was pin-rolled in [18, 20]. Both ends of chord were fixed in [21], and pin-rolled in [17]. The specimens were designed as shown in **Table 1** to evaluate the influence of different dimensionless geometric parameters, i.e. diameter ratio β (= d/D), diameter to thickness ratio of chord 2γ (= D/T) and thickness ratio τ (= t/T). The axial compressive or tensile force was applied to the hollow brace, which was fully welded at a right angle to the continuous concrete-filled chord. The static tests within elastic range were performed to obtain the HSS and the SCFs at weld toe of the specimens were determined.

2.2 FE models

The general purpose FE analysis software MSC.Marc was applied for the numerical investigation on SCF distribution of CFST T-joint under axial force in the brace. Since the measured HSS was much lower than yield stress in the experiment, linear elastic analysis in terms of material properties was conducted. The values of Young's modulus and Poisson's ratio were set to those shown in the article, as summarized in **Table 2**.

If the steel tube was modeled by shell element, it becomes difficult to model the weld bead and make good contact behavior between steel tube and concrete. Therefore, the linear full-integration eight-node hexahedron solid element was used for whole model, i.e. steel tube, concrete and weld bead. The leg sizes of weld bead at the brace and chord were set to t and $0.5t$ (t: the wall thickness of brace), respectively, according to AWS code [10].

Since the mesh size needs to be small enough to get the accurate HSS, fine mesh should be used around the intersection. The mesh dimensions of $0.5T$ to $0.5t$ around focused areas were suggested for solid element [22]. The influence of mesh size around the chord-brace intersection on the SCFs is examined in 2.4.

The behavior of the interface between chord tube and concrete can be simulated by "Glue" or "Touch" function. "Glue" function assumes that contact bodies tie together without any relative displacements. "Touch" function allows contact bodies to touch and separate each other in normal direction, and slide with the friction behavior in tangential direction. The function to be used is determined in 2.5. The whole FE model and local mesh around the intersection are shown in **Fig. 3**.

2.3 HSS calculation

The HSS around the chord-brace intersection was obtained numerically by linear extrapolation. The positions of two nodes for HSS calculation is shown in **Fig. 4** and **Table 3** [13]. The positions are arbitrarily determined in this region since the stress distribution is almost linear. In this study, the positions of 1st and 2nd nodes are approximately 0.4*T* (but ≥ 4 mm) and 1.0*T* away from the weld toe, respectively. The SCF is generally defined as the ratio of the HSS at the joint to the nominal stress in the member due to the basic member load causing this HSS [13]. Therefore, the nominal stress of the brace subjected to the axial force *F* was determined using a simple formula ($\sigma_n = F/A$), where *A* is the cross-sectional area of the brace [17], which was used for SCF calculation in this study.

2.4 Mesh size around chord-brace intersection

In order to determine the mesh size around the intersection, its influence on SCFs was examined. The three mesh conditions listed in **Table 4** were considered to calculate the SCFs of CFCHS-4 specimen in [17]. The influence of mesh size on SCFs for location CC under tensile or compressive axial force in the brace is shown in **Fig. 5**. It shows that the SCFs gradually increase as the mesh size decreases. Considering the balance between calculation accuracy and efficiency, the mesh size of approximately 2 mm was adopted in the parametric analysis.

2.5 Modeling of chord tube-concrete interface

The friction coefficient (μ) between concrete and steel is from 0.2 to 0.6 in general [23]. The SCFs at the chord crown under tensile force in the brace obtained by FE analysis with "Glue" and "Touch" functions assuming different friction coefficient in the range are compared with the test result of T-300-4 specimen [24] in **Fig. 6**. It shows that the SCFs calculated with "Glue" function are much lower than test result. However, the SCFs calculated with "Touch" function show good agreement with the test result and friction coefficient has almost no influence on the SCFs. Therefore, "Touch" function with μ = 0.3 was arbitrarily adopted in this study.

The relative deformations between chord and concrete around the chord-brace intersection are shown in **Fig. 7**. It is confirmed that total cross-section of chord and concrete bears the axial force in the brace with "Glue" function, while employing "Touch" function leads to separation between chord and filled-concrete around intersection.

2.6 Validation of the FE models

Fig. 8 shows a comparison of SCF distributions between FE analysis (SCF_{FEA}) and experiment (SCF_{Test}) for CFCHS-4 specimen in [17]. The developed FE model reproduces not only similar distribution but also similar magnitudes in SCFs.

Comparisons between the SCF_{FEA} and SCF_{Test} in four locations (chord saddle CS, chord crown CC, brace saddle BS and brace crown BC) and the maximum SCFs among four locations in each specimen are shown in **Fig. 9** for all specimens. The averages of SCF_{FEA} to SCF_{Test} ratio of the locations CS, CC, BS, BC and maximum SCFs location under tensile condition are 1.22, 0.95, 0.98, 0.79 and 0.97, respectively, and those under compressive condition are 0.96, 0.86, 0.86, 0.68 and 0.86, respectively. The SCF_{FEA} under tensile condition shows good agreement with the SCF_{Test} although they show larger deviation under compressive condition. The external surface of filled-concrete might have much smaller Young's modulus than design value in the actual specimen due to imperfect construction such as incomplete filling and generation of laitance. It would cause the larger measured SCFs than the calculated SCFs in FE model under compressive condition. However, it would hardly affect the measured SCFs under tensile condition because of the separation between chord tube and concrete around the intersection. Consequently, such difference in deviation has occurred between tensile and compressive conditions.

In order to examine the influence of such imperfect construction on the SCFs, CFCHS-4 specimen was analyzed assuming 0.5 and 0.1 times of Young's modulus for the concrete elements up to approximately 10mm deep from the surface. **Table 5** summarizes the results. It shows the great and slight influences of imperfect construction on the SCFs under compressive and tensile conditions, respectively. In other words, larger SCFs can be obtained under compression in the test if there is such imperfect construction.

The deviation of SCF_{FEA} at location BC is large not only under compressive condition, but also under tensile condition compared with the other locations. Therefore, it can be thought that some fabrication errors exist in the brace. For example, its plate thickness or diameter is less than design value and the angle between chord and brace is not 90°.

Based on the above discussions, it can be concluded that the developed FE models can predict the SCF distribution of CFST T-joint under axial loading in the brace with sufficient accuracy.

3 Parametric analysis on SCFs

3.1 FE models

Based on the SCF formulae of CHS T-joints [13] and the existing experimental results [17, 18], the diameter ratio β (= d/D), diameter to thickness ratio of chord 2γ (= D/T), thickness ratio τ (= t/T) and relative chord length α (= $2L/D$) are considered to be the key parameters for the determination of SCFs of CFST T-joints. Therefore, these four parameters were changed within the practical ranges shown in **Table 6** in the parametric analysis. The practical ranges were determined based on the geometric parameters statistics of CFST K-joint for 119 CFST trussed arch bridges in China [24].

The geometric dimensions of standard FE model, which was set referring to the common dimensions of CFST trussed arch bridges [1], are shown in **Table 7**. Two hundred and twelve FE models with different combination of geometric parameters were prepared and analyzed.

In general, the braces mainly bear axial forces and the chords bear axial compressive force and in-plane bending in the arch ribs of CFST trussed arch bridges. Therefore, CFST T-joints generally subject to axial force in the brace and axial force and in-plane bending in the chord, as shown in **Table 8**. In this study, only axial force in the brace was used as the loading condition to carry out the parametric analysis. In addition, the pinned chord ends and free brace end were employed in the FE models.

Young's modulus of steel tube and concrete were set to 2.05×10^5 MPa and 3.45×10^4 MPa, and their Poisson's ratio were set to 0.3 and 0.2, respectively. Wang [17] experimentally presented that the effect of concrete strength on the SCFs of CFST T-joints was not significant, even can be neglected. Since concrete with the strength between 30 and 60 MPa has been applied to the arch ribs of CFST arch bridges in China [1], the concrete of 50 MPa grade was assumed for the determination of Young's modulus of concrete [25].

3.2 Results and discussions

3.2.1 Influence of diameter ratio β

The influences of β on SCFs are illustrated in **Fig. 10**.

For the location CS (**Fig. 10 (a)**), the SCF_{CS} decreases as the value of β increases under tensile force. However, under compressive force, it increases for larger values of β.

For the location CC (**Fig. 10 (b)**), the SCF_{CC} increases as the value of β increases under tensile and compressive force.

For the location BS (**Fig. 10 (c)**), the SCF_{BS} decreases as the value of β increases from 0.3 to 0.5 under tensile force, but it increases as the value of β increases from 0.5 to 0.6. Moreover, it increases as the value of β increases under compressive force.

For the location BC (**Fig. 10 (d)**), the SCF_{BC} decreases as the value of β increases under tensile force. However, the influence of β on SCF_{BC} is not significant under compressive force.

3.2.2 Influence of diameter to thickness ratio of chord 2γ

The influences of 2γ on SCFs are illustrated in **Fig. 11**.

For the location CS (**Fig. 11(a)**), the SCF_{CS} increases as the value of 2γ increases under tensile force. However, it decreases as the value of 2γ increases under compressive force.

For the location CC (**Fig. 11(b)**), the SCF_{CC} increases as the value of 2γ increases under tensile force. However, it decreases as the value of β increases under compressive force.

For the location BS (**Fig. 11(c)**), the SCF_{BS} increases as the value of 2γ increases under tensile force. Moreover, it increases as the value of 2γ increases from 40 to 50 under compressive force, but it decreases as the value of 2γ increases from 50 to 80.

For the location BC (**Fig. 11(d)**), the SCF_{BC} decreases as the value of 2γ increases under tensile and compressive force.

3.2.3 Influence of thickness ratio τ

The influences of τ on SCFs are illustrated in **Fig. 12**.

For the location CS (**Fig. 12(a)**), the SCF_{CS} increases as the value of τ increases under tensile and compressive force.

For the location CC (**Fig. 12(b)**), the SCF_{CC} increases as the value τ increases under tensile and compressive force.

For the location BS (**Fig. 12(c)**), the SCF_{BS} increases as the value of τ increases under tensile force. Moreover, it increases as the value of τ increases from 0.4 to 0.7 under compressive force, but it decreases as the value of τ increases from 0.7 to 1.0.

For the location BC (**Fig. 12(d)**), the SCF_{BC} increases as the value of τ increases from 0.4 to 0.5 under tensile force, but it decreases as the value of τ increases from 0.5 to 1.0. In addition, it increases as the value of τ increases under compressive force.

3.2.4 Influence of relative chord length α

The influences of α on SCFs are illustrated in **Fig. 13**.

For the location CS (**Fig. 13(a)**), the influence of α on the SCF_{CS} can be neglected under tensile force. In addition, the influence is also not significant under compressive force.

For the location CC (**Fig. 13(b)**), the SCF_{CC} increases as the value of α increases under tensile and compressive forces.

For the location BS (**Fig. 13(c)**), the influence of α on the SCF_{BS} can be neglected under tensile force. Moreover, the influences of α is not significant under compressive force.

For the location BC (**Fig. 13(d)**), the influence of α on the SCF_{BC} can be neglected under tensile and compressive forces.

3.2.5 Discussions

By comparing the SCFs caused by tensile force with those caused by compressive force shown in **Figs. 10-13**, it can be noticed that the former is generally much larger than the latter. Since the adhesion between the steel and concrete was not strong, the inner wall of chord tube around the intersection tended to separate from the surface of filled-concrete when the brace was subjected to tensile force. Consequently, the out-of-plane bending deformation of the chord tube around the intersection became larger, which induced higher HSS under tensile force than under compressive force. In addition, the influence of τ on SCFs is much larger than that of β, 2γ and α for all four locations in most cases.

By comparing the SCF_{CS} with SCF_{CC}, it can be also noticed that the SCF_{CS} are larger under tensile force, while the SCF_{CC} are larger under compressive force in most cases. It indicates that the maximum SCFs in the chord generally occur at the saddle (CS) and crown (CC) under tensile and compressive force, respectively. Meanwhile, the maximum SCFs of CHS T-joints generally occur at location CS, regardless of whether the axial force applied to the brace is compression or tension [17]. The mechanical behavior around the intersection of CFST T-joints under tensile force is considered to be similar to that of CHS T-joints since the separation between chord tube and filled-concrete can occur in CFST T-joint. In contrast, the filled-concrete greatly increases the stiffness of CFST T-joint against compressive force in the brace and makes the stress distribution around the intersection more uniform. Furthermore, the position of the maximum SCFs changed from the saddle (CS) to crown (CC).

By comparing the SCF_{BS} with SCF_{BC}, it can be noticed that the SCF_{BS} are generally larger under tensile force, while the magnitudes of SCF_{BS} and SCF_{BC} are similar under compressive force. In other words, the maximum SCFs in the brace occur at the saddle (BS) under tensile force in general. However, they can occur at the saddle (BS) or crown (BC) under compressive force. The difference of maximum SCF location in the brace can be explained similarly to the above discussions.

4 SCF formulae for CFST T-joints

4.1 Formulation

Based on the results of parametric analysis as well as the SCF formulae given in the CIDECT Design Guide [13] for CHS T-joints subjected to axial force in the brace, the SCF formulae at locations CS and CC under tensile or compressive force can be expressed as **Eqs. (1)** and **(2)**, respectively. Those at locations BS and BC under tensile and compressive force can be expressed as **Eqs. (3)** and **(4)**, respectively.

The axial loading in the brace results in a bending moment in the chord. The bending moment is the main cause of the stress at location CC, and it changes with chord length which can be represented by α. Therefore, the influence of α on SCFs at location CC needs to be considered. Referring to [26], the last term corresponding to the SCF at location CC due to global bending is introduced in **Eq. (2)**. The direction of stress caused by the bending moment in the chord is the longitudinal direction along the chord tube and perpendicular to the weld toe at location CC, while parallel to the weld toe at location CS. Therefore, the influence of α on SCFs at location CS is not considered in **Eq. (1)**.

$$\mathrm{SCF_{CS}} = A_{\mathrm{CS}} \cdot \gamma^{B_{\mathrm{CS}}} \cdot \tau^{C_{\mathrm{CS}}} \cdot [D_{\mathrm{CS}} + E_{\mathrm{CS}} \cdot (\beta + F_{\mathrm{CS}})^2] \tag{1}$$

$$\mathrm{SCF_{CC}} = A_{\mathrm{CC}} \cdot \gamma^{B_{\mathrm{CC}}} \cdot \tau^{C_{\mathrm{CC}}} \cdot [D_{\mathrm{CC}} + E_{\mathrm{CC}} \cdot (\beta + F_{\mathrm{CC}})^2] + \frac{M_{\mathrm{Chord}}}{W_e \sigma_n} \tag{2}$$

$$\mathrm{SCF_{BS}} = A_{\mathrm{BS}} \cdot \gamma^{B_{\mathrm{BS}}} \cdot \tau^{C_{\mathrm{BS}}} \cdot [D_{\mathrm{BS}} + E_{\mathrm{BS}} \cdot (\beta + F_{\mathrm{BS}})^2] \quad \text{(tension)} \tag{3a}$$

$$= A_{\mathrm{BS}} \cdot \gamma^{B_{\mathrm{BS}}} \cdot \beta^{C_{\mathrm{BS}}} \cdot [D_{\mathrm{BS}} + E_{\mathrm{BS}} \cdot (\tau + F_{\mathrm{BS}})^2] \quad \text{(compression)} \tag{3b}$$

$$\mathrm{SCF_{BC}} = A_{\mathrm{BC}} \cdot \gamma^{B_{\mathrm{BC}}} \cdot \beta^{C_{\mathrm{BC}}} \cdot [D_{\mathrm{BC}} + E_{\mathrm{BC}} \cdot (\tau + F_{\mathrm{BC}})^2] \quad \text{(tension)} \tag{4a}$$

$$= A_{\mathrm{BC}} \cdot \gamma^{B_{\mathrm{BC}}} \cdot \tau^{C_{\mathrm{BC}}} \cdot \beta^{D_{\mathrm{BC}}} \quad \text{(compression)} \tag{4b}$$

where, the constants A_{CS} to F_{CS}, A_{CC} to F_{CC}, A_{BS} to F_{BS} and A_{BC} to F_{BC} would be determined by multiple regression analysis. M_{Chord} is the global bending moment in the chord around the intersection, W_{e} is the section modulus for equivalent steel tube section, and σ_{n} is the nominal stress in the brace.

Assuming a small wall thickness compared with the diameter of brace, the relation between the force F and the nominal stress in the brace (σ_{n}) is derived as follows.

$$F = \pi d t \sigma_{\mathrm{n}} \tag{5}$$

The flexural stiffness EI of concrete-filled chord is determined according to the **Eq. (6)** [27].

$$EI = E_c I_c + E_s I_s \tag{6}$$

where, E_{c} and E_{s}, I_{c} and I_{s} are the Young's moduli and moments of inertia of filled-concrete and steel tube, respectively.

The moment of inertia of steel tube and filled-concrete are calculated by **Eqs. (7)** and **(8)**, respectively.

$$I_s = \frac{\pi[D^4 - (D-2T)^4]}{64} \tag{7}$$

$$I_c = \frac{\pi(D-2T)^4}{64} \tag{8}$$

From **Eqs. (6)-(8)**, the wall thickness T_e of the equivalent steel tube section is derived as follows.

$$T_e = \frac{D-(D-2T)\cdot\sqrt[4]{\frac{m-1}{m}}}{2} \tag{9}$$

$$m = \frac{E_s}{E_c} \tag{10}$$

Consequently, the section modulus for equivalent steel tube section W_e is obtained as follows.

$$W_e = \frac{\pi D^3}{32}(1-n^4) \tag{11}$$

$$n = \frac{D-2T_e}{D} \tag{12}$$

According to the results of the multiple regression analysis, the formulae for determining SCFs in the chord and brace of CFST T-joints under axial force in the brace are given as follows,

Location CS

$$\mathrm{SCF_{CS}} = 2.351\gamma^{0.39}\tau^{1.03}[0.818+1.254(\beta-0.878)^2] \quad \text{(tension)} \quad (13a)$$

$$= 6.767\gamma^{-0.482}\tau^{0.79}[0.984+1.255(\beta-0.198)^2] \quad \text{(compression)} \quad (13b)$$

Location CC

$$\mathrm{SCF_{CC}} = 1.401\gamma^{0.365}\tau^{0.916}[1.028 + 0.883(\beta - 0.29)^2] + \frac{M_{\mathrm{Chord}}}{W_e \sigma_n} \quad \text{(tension)} \quad (14a)$$

$$= 37.077\gamma^{-1.096}\tau^{0.895}[1.122 - 0.095(\beta + 0.274)^2] + \frac{M_{\mathrm{Chord}}}{W_e \sigma_n} \quad \text{(compression)} \quad (14b)$$

Location BS

$$\mathrm{SCF_{BS}} = 0.636\gamma^{0.308}\tau^{0.28}[2.751 + 8.645(\beta - 0.531)^2] \quad \text{(tension)} \quad (15a)$$

$$= 0.989\gamma^{-0.044}\beta^{0.316}[2.942 - 0.638(\tau - 0.759)^2] \quad \text{(compression)} \quad (15b)$$

Location BC

$$\mathrm{SCF_{BC}} = 1.122\gamma^{-0.228}\beta^{-0.317}[3.154 - 3.121(\tau - 0.519)^2] \quad \text{(tension)} \quad (16a)$$

$$= 6.025\gamma^{-0.329}\tau^{0.326}\beta^{-0.007} \quad \text{(compression)} \quad (16b)$$

The validity ranges of the proposed parametric formulae in **Eqs. (13)-(16)** are $0.3 \leq \beta \leq 0.6$, $40 \leq 2\gamma \leq 80$, $0.4 \leq \tau \leq 1.0$ and $12 \leq \alpha \leq 20$ since the validity of the formulae has been confirmed only for those ranges.

4.2 Accuracy verification

The SCFs obtained by the proposed formulae, $\mathrm{SCF_{FOR}}$, were compared with those by FEA, $\mathrm{SCF_{FEA}}$, for all locations to verify the accuracy of the formulae. The comparisons under axial tensile force and compressive force are shown in **Figs. 14(a)-(d)** and **Figs. 14(e)-(h)**, respectively. They include the statistical values of the ratio of $\mathrm{SCF_{FOR}}$ to $\mathrm{SCF_{FEA}}$, $\mathrm{SCF_{FOR}}/\mathrm{SCF_{FEA}}$, as well. The graphs show the good agreement between $\mathrm{SCF_{FOR}}$ and $\mathrm{SCF_{FEA}}$ in general. The mean values of $\mathrm{SCF_{FOR}}/\mathrm{SCF_{FEA}}$ are very close to 1.0 for all locations, and the corresponding coefficients of variance (COV) are relatively small.

However, conspicuous disagreements and different trends are observed at locations CS and BS under compressive axial force. In order to examine the reason, **Figs. 14(e)** and **(g)** are divided into three graphs by α-value, respectively, as shown in **Fig. 15**. Then, most different trends disappear. It indicates that the different trends are mainly caused by ignoring the influence of α-value in the developed formulae for locations CS and BS. Although the accuracy can be improved by considering the influence of α-value, the authors do not think that it is necessary due to much smaller SCFs than those at the same locations under tension.

Therefore, it can be concluded that the proposed SCFs formulae have sufficient accuracy and reliability for CFST T-joints under axial force in the brace.

5 Conclusions

This study focuses on the SCFs of CFST T-joints under axial force in the brace. The validity of the developed FE models was evaluated by comparison with the existing experimental results. Parametric analysis was conducted by using the validated FE model to reveal the effects of the key four non-dimensional geometric parameters (β, 2γ, τ and α) on the SCFs. Based on the numerical results from 424 FE analyses, a series of parametric formulae were proposed to determine the SCFs of CFST T-joints under axial force in the brace. The main conclusions are summarized as follows.

(1) The developed three-dimensional FE models can determine the HSS at the chord-brace intersection under axial force in the brace with sufficient accuracy.

(2) The influence of non-dimensional geometric parameters (β, 2γ, τ and α) on SCFs of CFST T-joints under axial force in the brace can be summarized as shown in **Table 9**. Moreover, the influence of τ on the SCFs is much larger than that of β, 2γ and α for all four locations in most cases.

(3) The SCFs in the chord caused by axial tensile force are much larger than those under compression. The maximum SCFs in the chord generally occur at locations CS and CC under axial tensile and compressive force, respectively. The maximum SCFs in the brace occur at location BS under axial tensile force in general. However, they can occur at locations BS or BC under axial compressive force.

(4) Using multiple regression analysis, parametric formulae to determine the SCFs for CFST T-joints under axial force in the brace were developed. Sufficient accuracy and reliability of the proposed formulae were demonstrated by comparison with FE analysis results.

As described in 4.1, the validity range of each parameter for the formulae is set to the same as that in the parametric analysis. Examination of the applicability of the parametric formulae for wider range of the parameters can be one of the future work.

Acknowledgments This research was financially supported by the National Natural Science Funds for Distinguished Young Scholar (No. 51408132) and China Scholarship Council (No. 201506650004).

References

[1] Wang Q, Nakamura S, Chen KM, Chen BC and Wu QX. Comparison between

steel and concrete-filled steel tubular arch bridges in China. Proceedings of constructional steel, Japanese Society of Steel Construction, 2016; 24: 66-73.

[2] Wang Q, Nakamura S, Chen KM, Chen BC and Wu QX. Fatigue evaluation of K-joint in a half-through concrete-filled steel tubular trussed arch bridge in china by hot spot stress method. Proceedings of constructional steel, Japanese Society of Steel Construction, 2016; 24: 633-640.

[3] Kuang JG, Potvin AB, Leick RD. Stress concentration in tubular joints. In: Proceedings of the seventh annual offshore technology conference, OTC 2205. Houston, Texas, 1975, p. 593-612.

[4] Efthymiou M, Durkin S. Stress concentrations in T/Y and gap/overlap K-joints. In: Behavior of offshore structures: proceedings of the 4th International Conference on Behavior of Offshore Structures. Amsterdam: Elsevier; 1985, p. 429-440.

[5] Hellier AK, Connolly MP, Dover WD. Stress concentration factors for tubular Y-and T-joints. International Journal of Fatigue 1990; 12(1): 13-23.

[6] Smedley PA, and Fisher PJ. Stress concentration factors for simple tubular joints. In: Proceedings of the first international offshore and polar engineering conference. International Society of Offshore and Polar Engineers, Edinburgh, UK, 1991, p. 475-483.

[7] Mashiri FR, Zhao XL, Grundy P. Stress concentration factors and fatigue behaviour of welded thin-walled CHS–SHS T-joints under in-plane bending. Engineering Structures 2004; 26(13): 1861-1875.

[8] Zhao XL, Wilkinson T, Hancock GJ. Cold-formed tubular members and

connections: Structural behaviour and design. Elsevier, Oxford, UK, 2005.

[9] API. American Petroleum Institute. Recommended practice for planning, designing and constructing fixed offshore platforms. 21th Ed., API Publishing Services, Washington DC, 2014.

[10] AWS. American Welding Society. Structural welding code-steel. AWS *D1.1/1.1M*. American Welding Society, Inc., Miami, 2004.

[11] ABS. American Bureau of Shipping. Guide for buckling and ultimate strength assessment for offshore structures. American Bureau of Shipping, Houston, 2004.

[12] DNV. DNV recommended practice RP-C203. Fatigue strength analysis of offshore of steel structures. Det Norske Veritas, Norway, 2010.

[13] Zhao XL, Herion S, Packer JA, Puthli R, Sedlacek G, Wardenier J. et al. Design guide for circular and rectangular hollow section joints under fatigue loading, CIDECT, TUV, 2000.

[14] JTG/T D65-06-2015. Specifications for design of highway concrete-filled steel tubular arch bridge. China Communication Press, Beijing, China, 2015 (in Chinese).

[15] Tong LW, Sun CQ, Chen YY, Zhao XL, Shen B and Liu CB. Experimental comparison in hot spot stress between CFCHS and CHS K-joints with gap. In: Proceedings of 12th International Symposium on Tubular Structures. 2008, p. 389-395.

[16] Mashiri FR, Zhao XL. Square hollow section (SHS) T-joints with concrete-filled

chords subjected to in-plane fatigue loading in the brace. Thin-Walled Structures 2010; 48(2): 150-158.

[17] Wang K, Tong LW, Zhu J, Zhao XL, Mashiri FR. Fatigue behavior of welded T-joints with a CHS brace and CFCHS chord under axial loading in the brace. Journal of Bridge Engineering 2011; 18(2): 142-152.

[18] Chen J, Chen J, Jin WL. Experiment investigation of stress concentration factor of concrete-filled tubular T joints. Journal of Constructional Steel Research 2010; 66(12): 1510-1515.

[19] Wang K. Study on the hot spot stress and fatigue strength of welded circular hollow section (CHS) T-joints with concrete-filled chords. Ph.D. thesis, Tongji Univ., Shanghai, China, 2008 (in Chinese).

[20] Chen J. Experimental and theoretical study of dynamic performance of concrete-filled steel tubular T-joints. Ph.D. thesis, Zhejiang Univ., Hangzhou, China, 2011 (in Chinese).

[21] Xu F, Chen J, Jin WL. Experimental investigation of SCF distribution for thin-walled concrete-filled CHS joints under axial tension loading. Thin-Walled Structures 2015; 93: 149-157.

[22] Herion S. Multiplanar K-joints made of RHS. Ph.D. thesis, University of Karlsruhe, Germany, 1994 (in German).

[23] Baltay P, Gjelsvik A. Coefficient of friction for steel on concrete at high normal stress. Journal of Materials in Civil Engineering 1990; 2(1): 46-49.

[24] Zheng J, Nakamura S, Chen KM, Wu QX. Numerical Parameter Analysis on

Stress Concentration Factors of Concrete-filled Steel Tubular (CFST) K-joint under Axial Loading. In: Proceedings of the 2017 World Congress on Advances in Structural Engineering and Mechanics. Seoul, Korea, 2017.

[25] JTG D62-2004. Code for design of highway reinforced concrete and prestressed concrete bridges and culverts. China Communication Press, Beijing, China, 2004 (in Chinese).

[26] Lotsberg I. On stress concentration factors for tubular Y-and T-Joints in frame structures. Marine Structures 2011; 24(1): 60-69.

[27] Chen BC. Concrete filled steel tubular arch bridges. China Communications Press, Beijing, China, 2007 (in Chinese).

Table 1 Details of test specimens

Ref. No.	Specimen	D (mm)	T (mm)	d (mm)	t (mm)	β	2γ	τ
[18, 20]	CS-203-133AX	203	8.45	133	6.80	0.66	24.02	0.80
	CS-203-159AX	203	8.42	159	6.81	0.78	24.11	0.81
[21]	T-300-4	299.84	4.19	132.78	6.08	0.443	75	1.5
	T-300-4R	300.11	4.18	133.25	6.08	0.443	75	1.5
	T-300-5	300.46	5.01	132.66	6.08	0.443	60	1.2
[17]	CFCHS-1	245	8	133	8	0.54	30.62	1.00
	CFCHS-2	180	6	133	6	0.74	30.00	1.00
	CFCHS-3	133	4.5	133	4.5	1.00	29.56	1.00
	CFCHS-4	245	8	133	6	0.54	30.62	0.75
	CFCHS-5	245	8	133	4.5	0.54	30.62	0.56
	CFCHS-6	245	8	133	8	0.54	30.62	1.00
	CFCHS-7	245	8	133	8	0.54	30.62	1.00
	CFCHS-8	203	8	140	8	0.69	25.38	1.00
	CFCHS-9	203	10	140	10	0.69	20.30	1.00
	CFCHS-10	203	12	140	12	0.69	16.92	1.00

Table 2 Material Properties for FE models

Ref. No.	Steel tube and weld bead		Concrete	
	Young's modulus (MPa)	Poisson's ratio	Young's modulus (MPa)	Poisson's ratio
[18, 20, 21]	200,000	0.3	37,420	0.2
[17]	205,000	0.3	34,500	0.2

Table 3 Boundaries of extrapolation region

Distance from weld toe	Chord		Brace
	Saddle	Crown	Saddle / Crown
Lr,min	0.4T, but ≥ 4 mm		0.4t, but ≥ 4 mm
Lr,max	0.045D	$0.4\sqrt[4]{0.25DTdt}$	$0.65\sqrt{0.5dt}$

Table 4 The mesh conditions

Mesh condition	Mesh size of solid element around intersection	Mesh layers in the thickness direction of steel tube
1 mm	Approximately 1 mm	Determining so that the edge length ratio of elements around the intersection is approximately 1.
2 mm	Approximately 2 mm	
0.5T (0.5t)	4 mm (3 mm)	Two layers

Table 5 Influence of Young's modulus of concrete surface on SCFs

Young's modulus	Conditions	SCFs			
		CC	CS	BC	BS
$0.1E_c$	Tension	4.60	3.73	1.76	3.10
	Compression	4.05	1.98	2.58	1.75
$0.5E_c$	Tension	4.56	3.62	1.75	2.87
	Compression	2.98	1.56	2.16	1.48
$1.0E_c$	Tension	4.33	3.49	1.72	2.78
	Compression	2.44	1.38	1.97	1.43

Table 6 Practical ranges of each parameter

Parameter	β	2γ	τ	α
Practical range	0.3 – 0.6	40 – 80	0.4 – 1.0	12 – 20

Table 7 Geometric parameters of standard FE model

Structural dimensions					
D/mm	d/mm	T/mm	t/mm	L/mm	l/mm
600	300	12	12	3600	900
Non-dimensional geometric parameters					
β	2γ	τ	α		
0.5	50	1.0	12		

Table 8 Combination of loading conditions

Load condition	
Axial force in brace	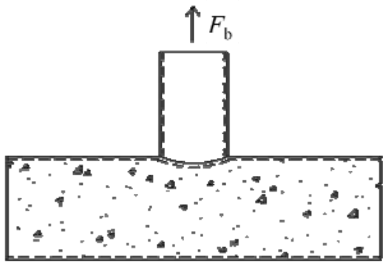
Axial force in chord	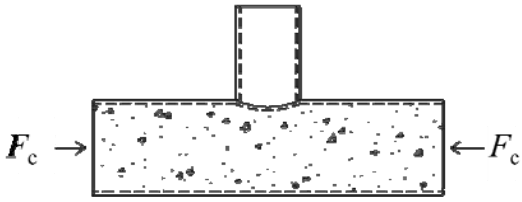
In-plane bending in chord	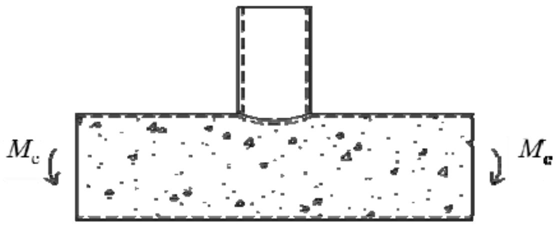

Table 9 Influence of geometric parameters on SCFs of CFST T-joints

Parameters		Chord				Brace			
		Saddle (CS)		Crown (CC)		Saddle (BS)		Crown (BC)	
		Tension	Comp.	Tension	Comp.	Tension	Comp.	Tension	Comp.
β	0.3→0.6	↘	↗	↗	↗	↘↗	↗	↘	–
2γ	40→80	↗	↘	↗	↘	↗	↗↘	↘	↘
τ	0.4→1.0	↗	↗	↗	↗	↗	↗↘	↗↘	↗
α	12→20	–	–	↗	↗	–	–	–	–

Where, "→" represents change from one value to other value, "↗" represents increasing, "↘" represents decreasing, "↗↘" represents increasing first and then decreasing, "↘↗" represents decreasing first and then increasing, and "–" represents almost constant.

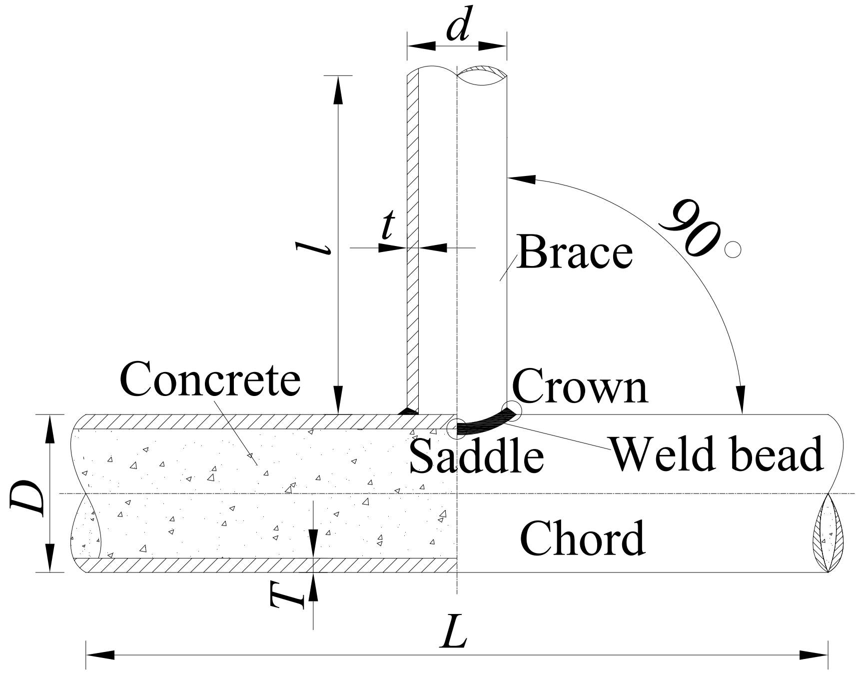

Fig. 1 Geometric parameters of CFST T-joints

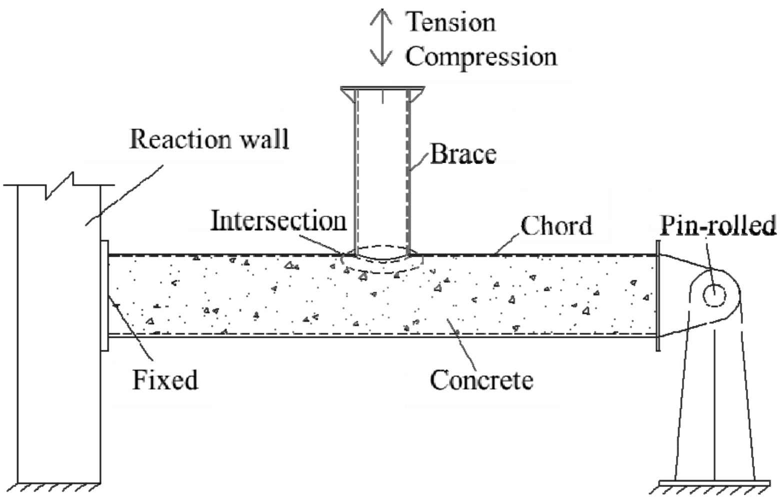

(a) Loading method in [18, 20]

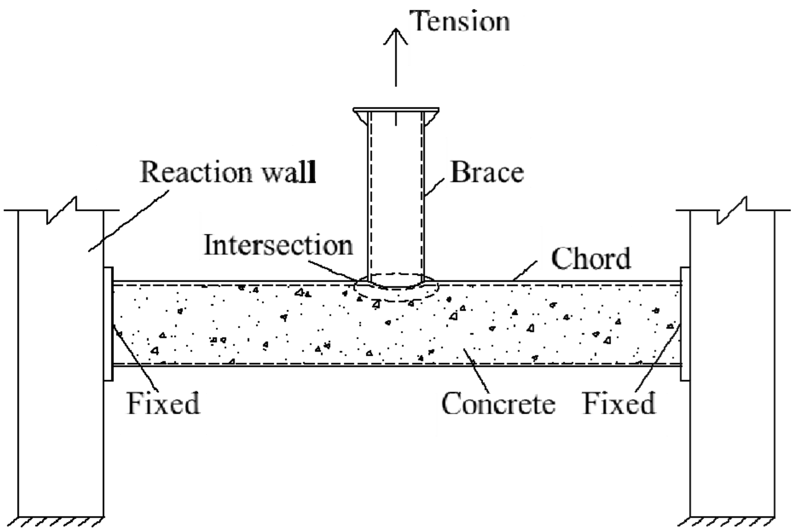

(b) Loading method in [21]

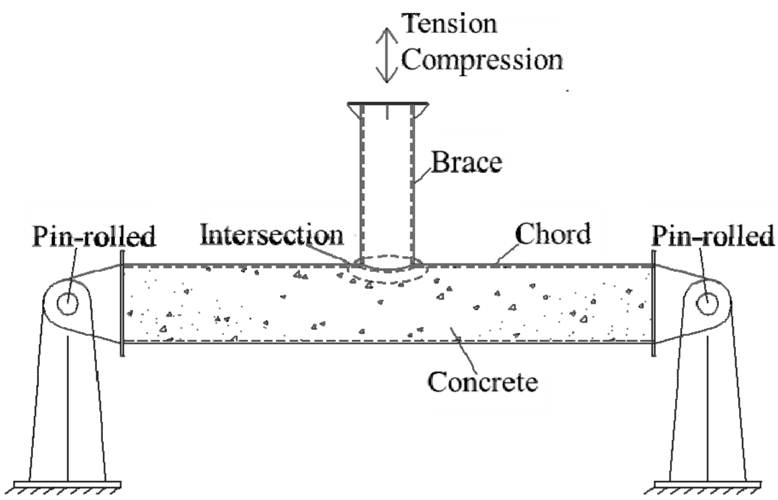

(c) Loading method in [17]

Fig. 2 Loading methods in literatures

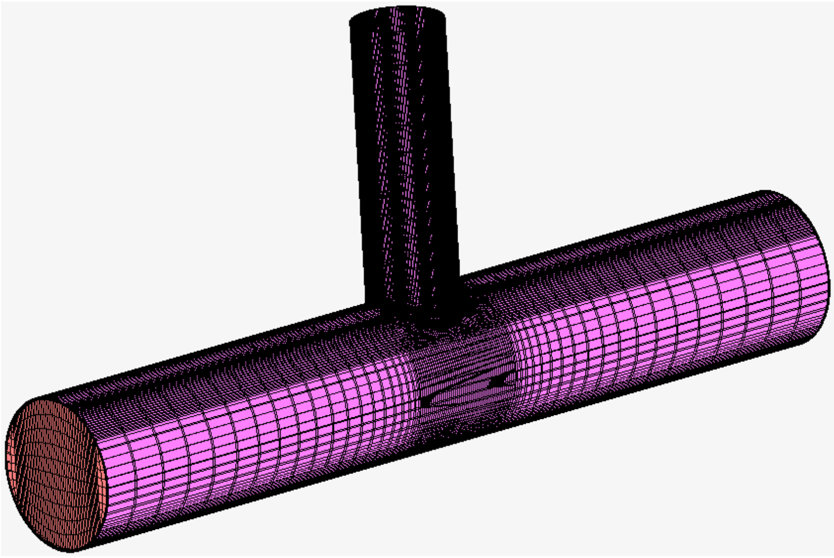

(a) FE model

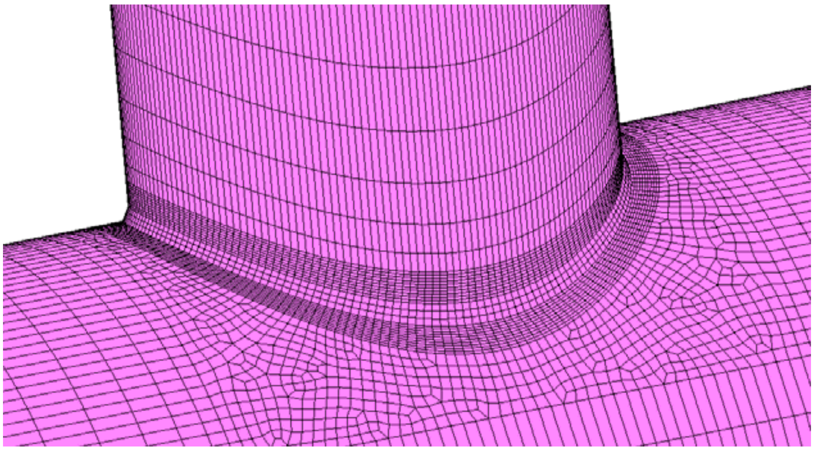

(b) Local mesh around the intersection

Fig. 3 FE model and local mesh of CFST T-joint

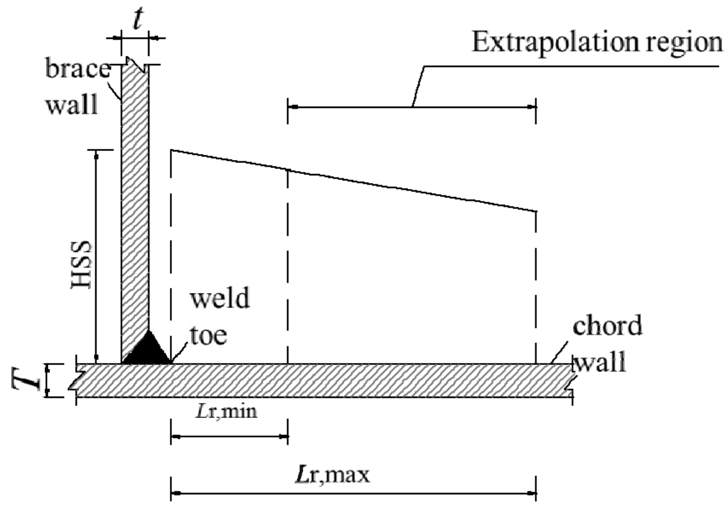

Fig. 4 Definition of extrapolation region

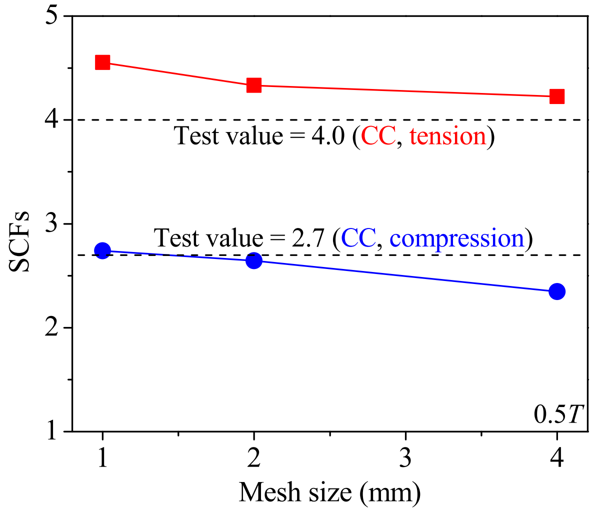

Fig. 5 Influence of mesh size on SCFs

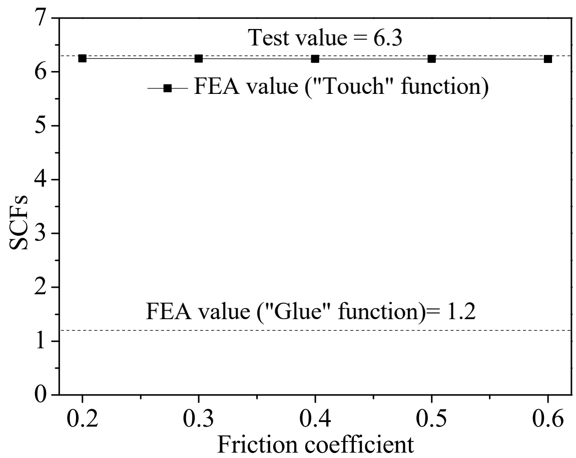

Fig. 6 Comparison of SCFs between "Touch" and "Glue" functions

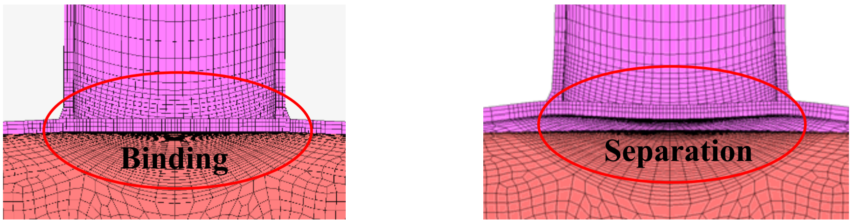

(a) “Glue” function (b) “Touch” function

Fig. 7 Comparison of deformation

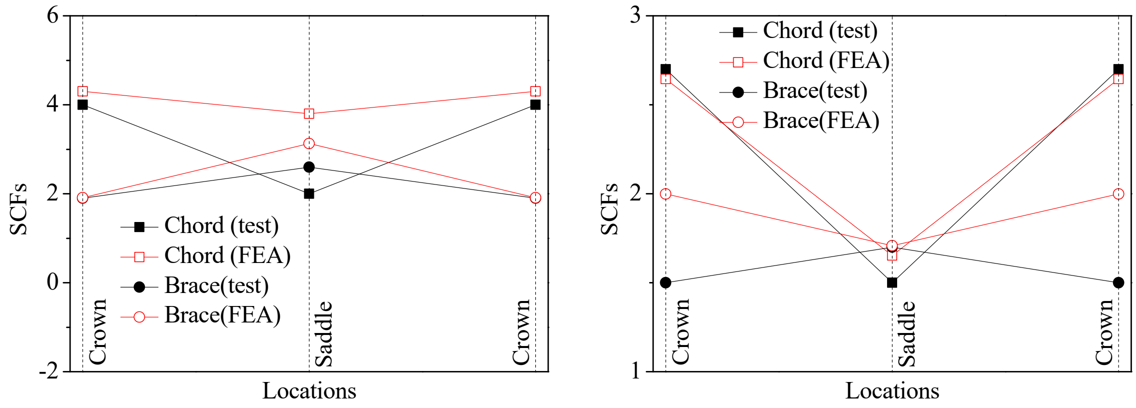

(a) CFCHS-4 (tension) (b) CFCHS-4 (compression)

Fig. 8 Comparison on SCFs distribution

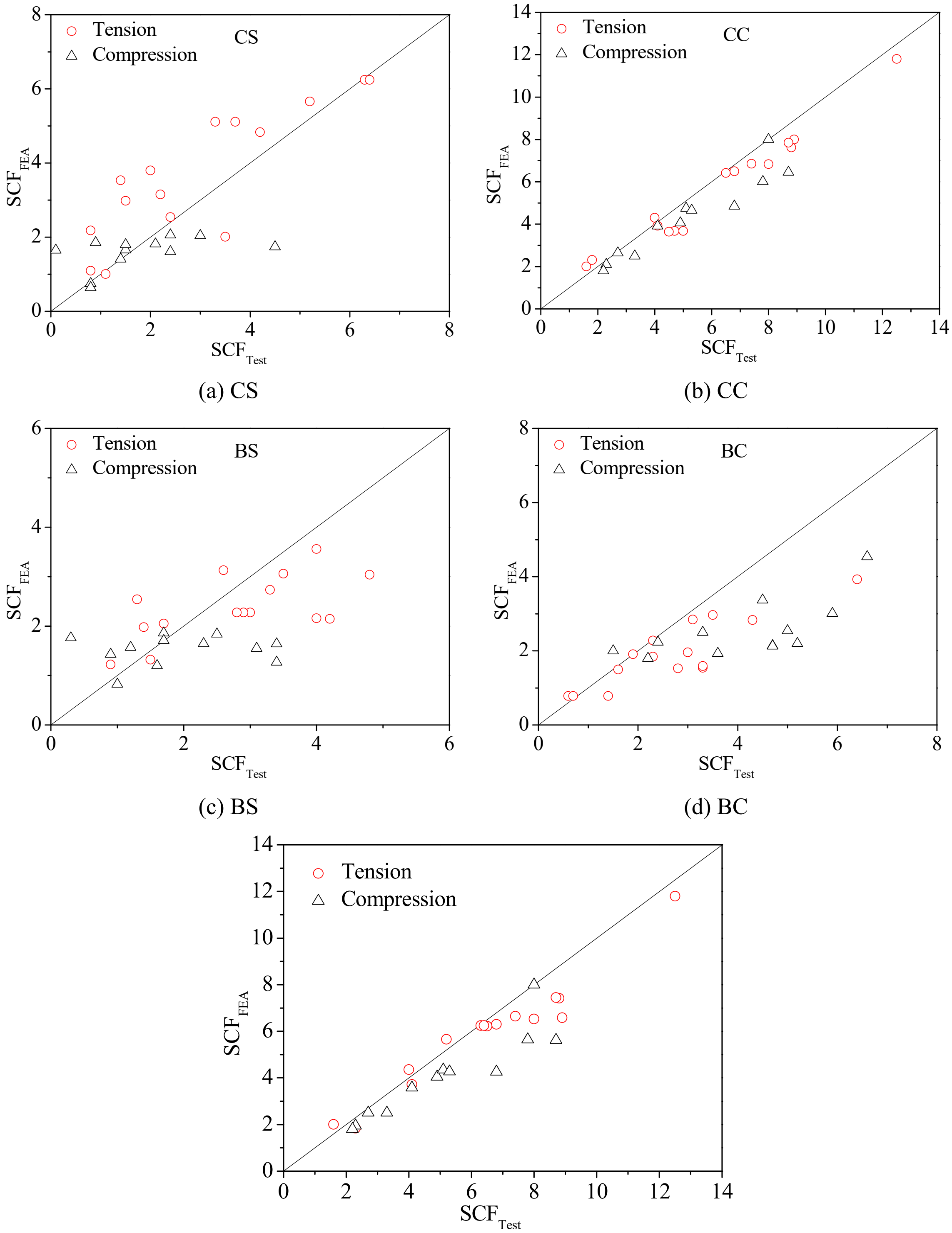

(e) Maximum SCFs

Fig. 9 Comparison on SCF_{FEA} with SCF_{Test}

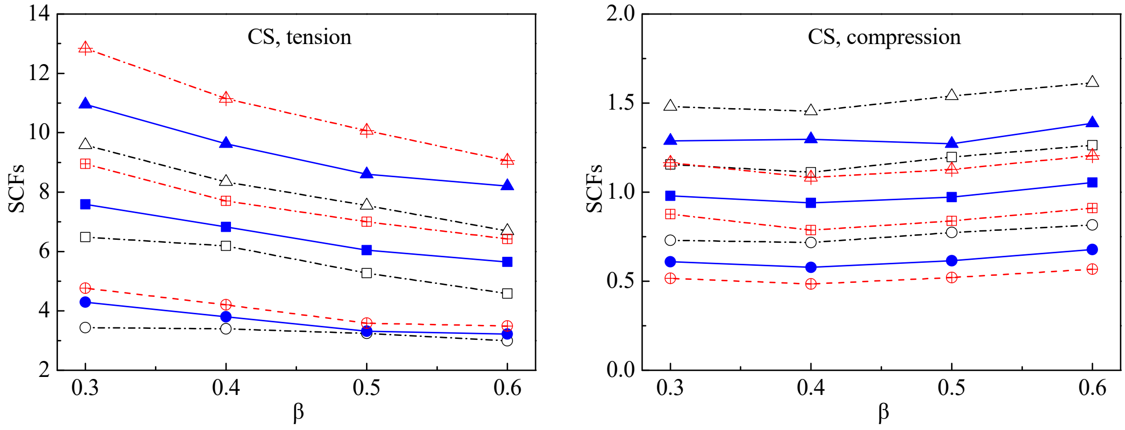

(a) SCF_{CS} vs. β

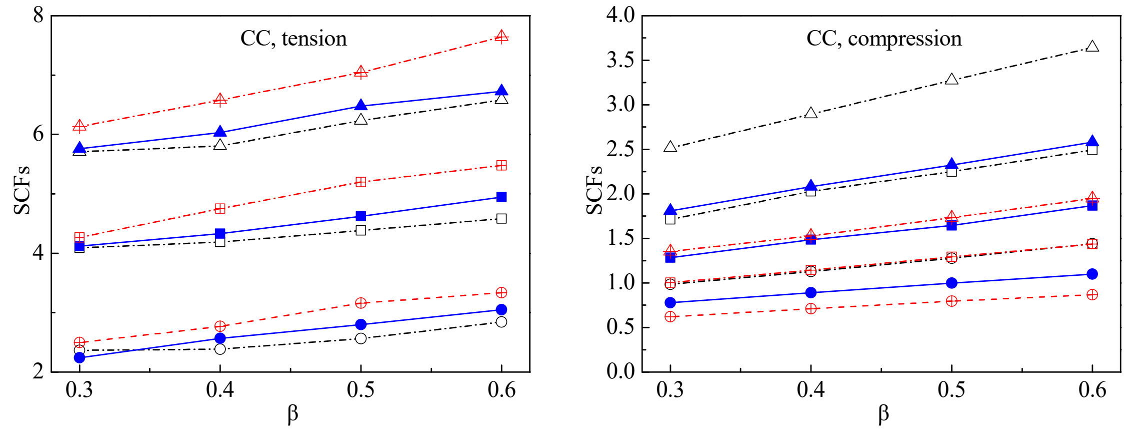

(b) SCF_{CC} vs. β

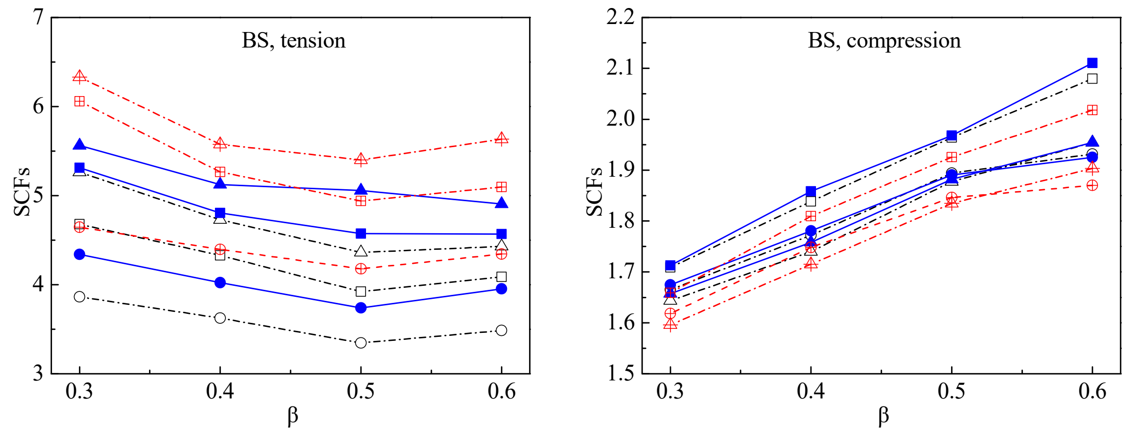

(c) SCF_{BS} vs. β

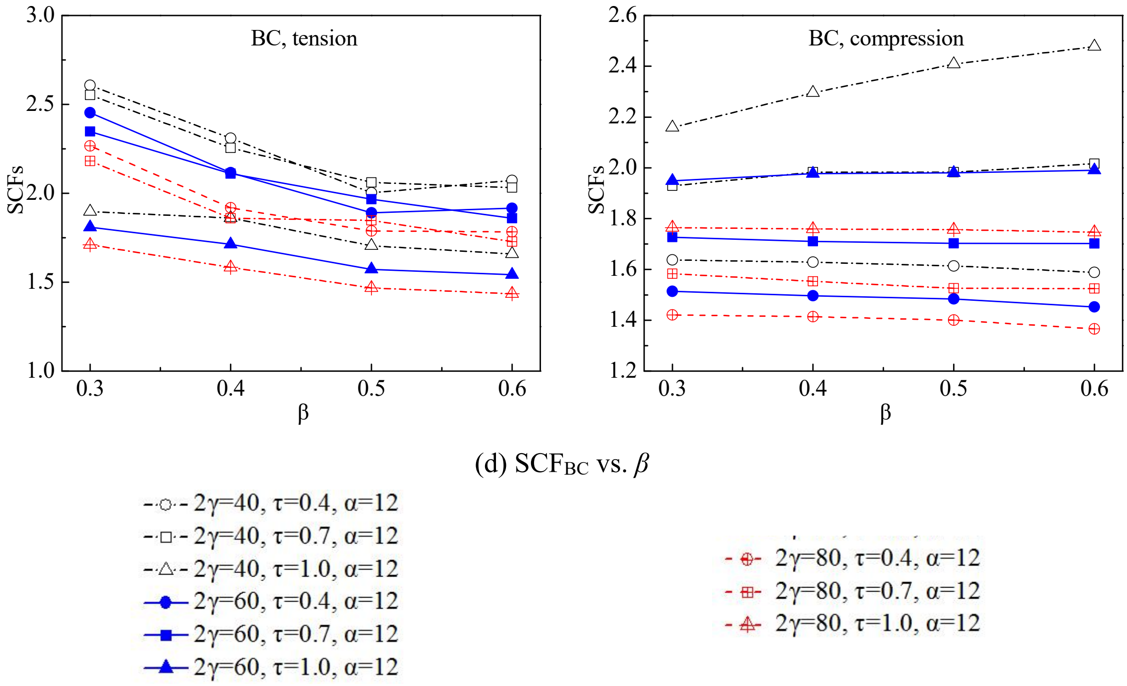

(d) SCF_{BC} vs. β

Fig. 10 Influence of β on SCFs under axial tensile and compressive force in the brace

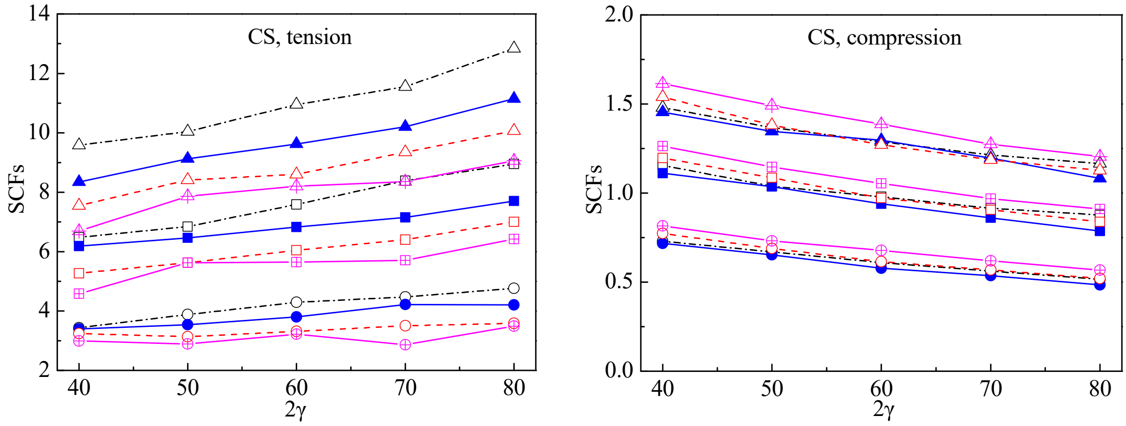

(a) SCF_{CS} vs. 2γ

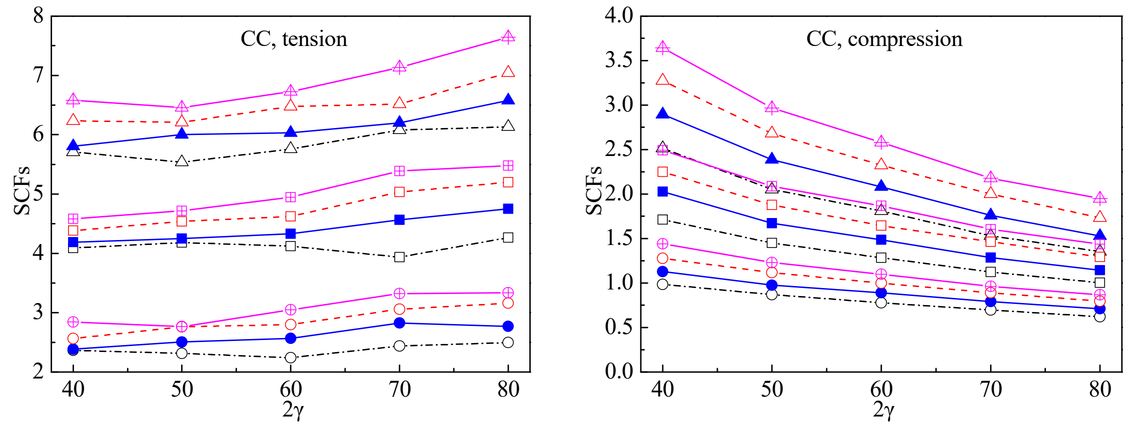

(b) SCF_{CC} vs. 2γ

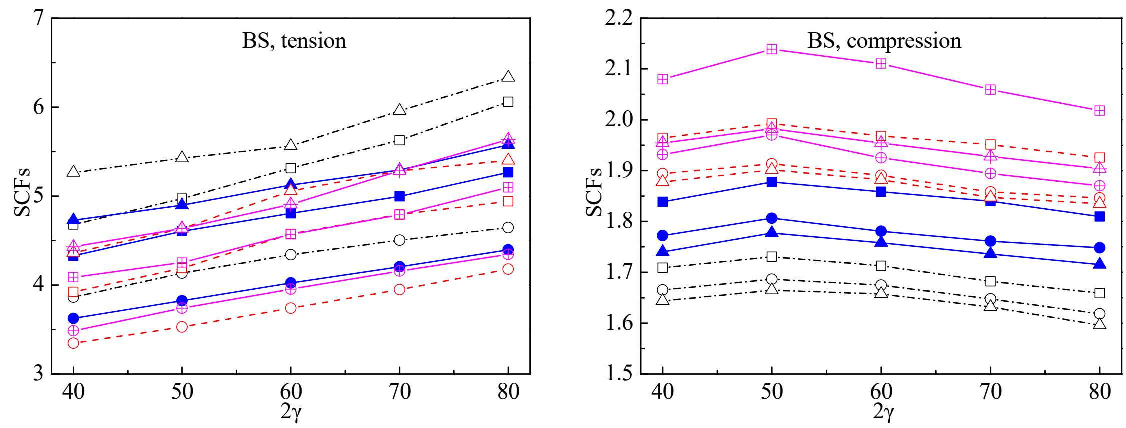

(c) SCF_{BS} vs. 2γ

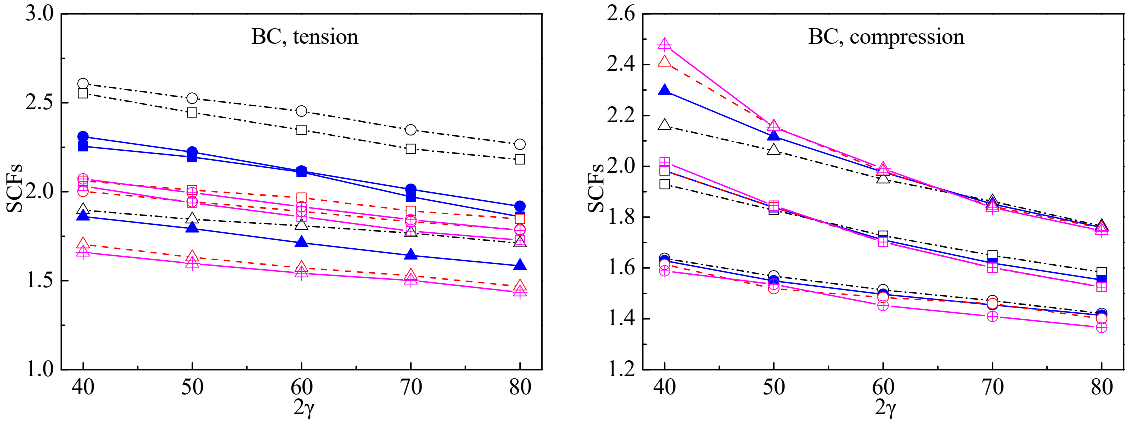

(d) SCF_{BC} vs. 2γ

Fig. 11 Influence of 2γ on SCFs under axial tensile and compressive force in the brace

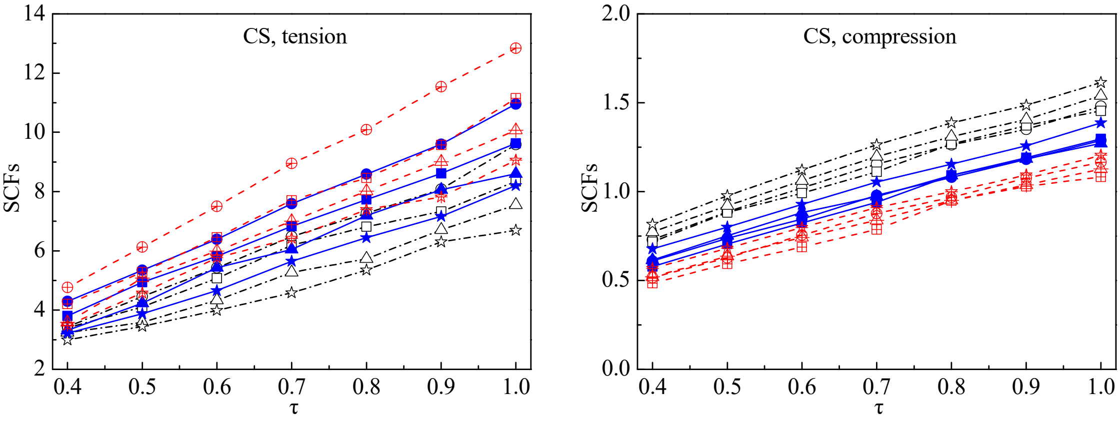

(a) SCF_{CS} vs. τ

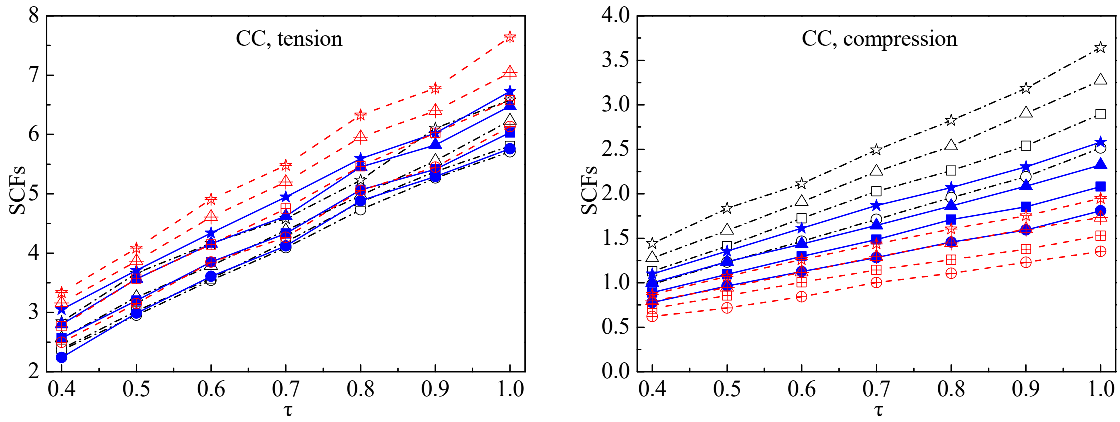

(b) SCF_{CC} vs. τ

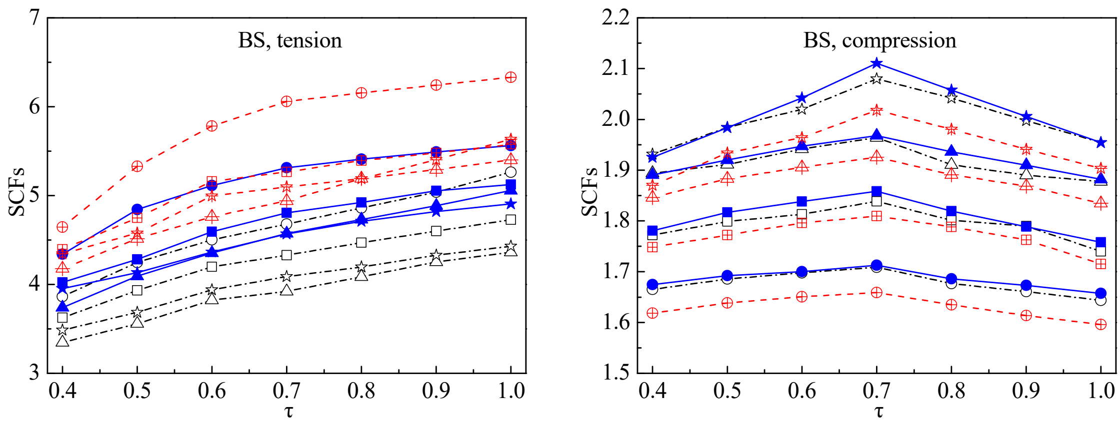

(c) SCF_{BS} vs. τ

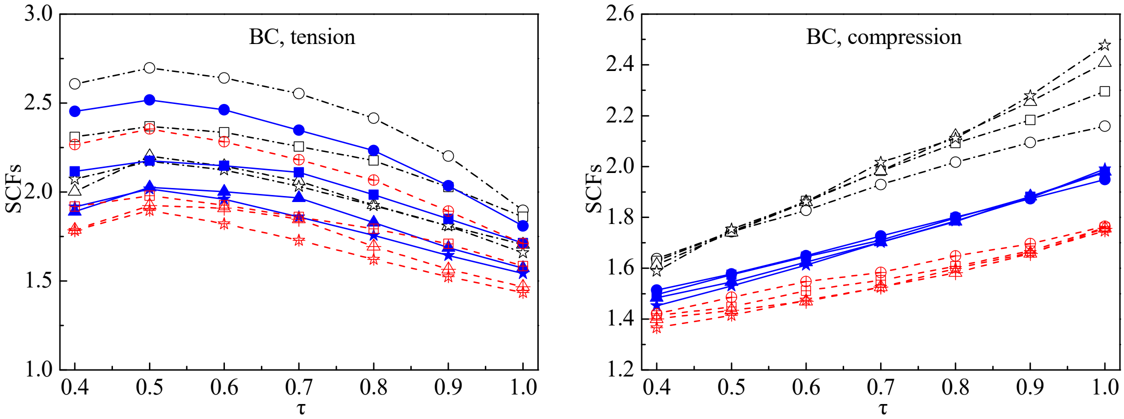

(d) SCF_{BC} vs. τ

Fig. 12 Influence of τ on SCFs under axial tensile and compressive force in the brace

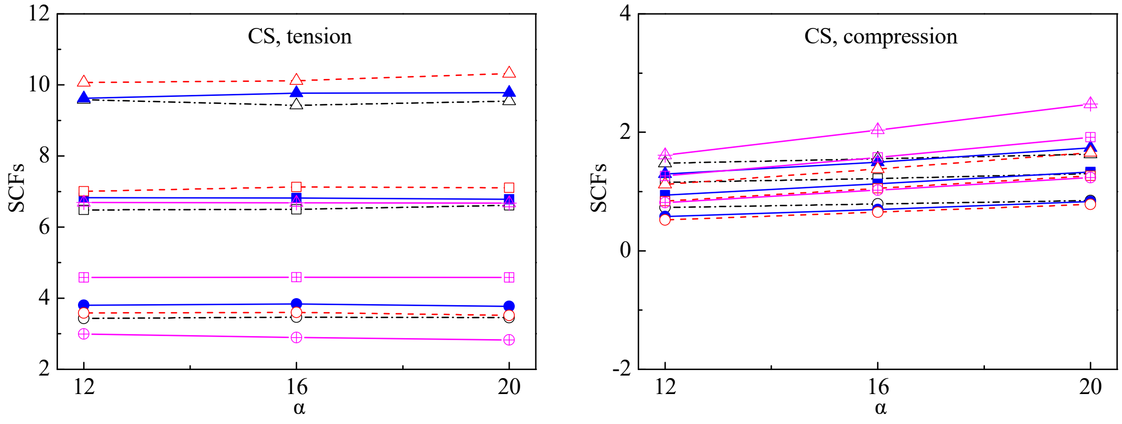

(a) SCF_{CS} vs. α

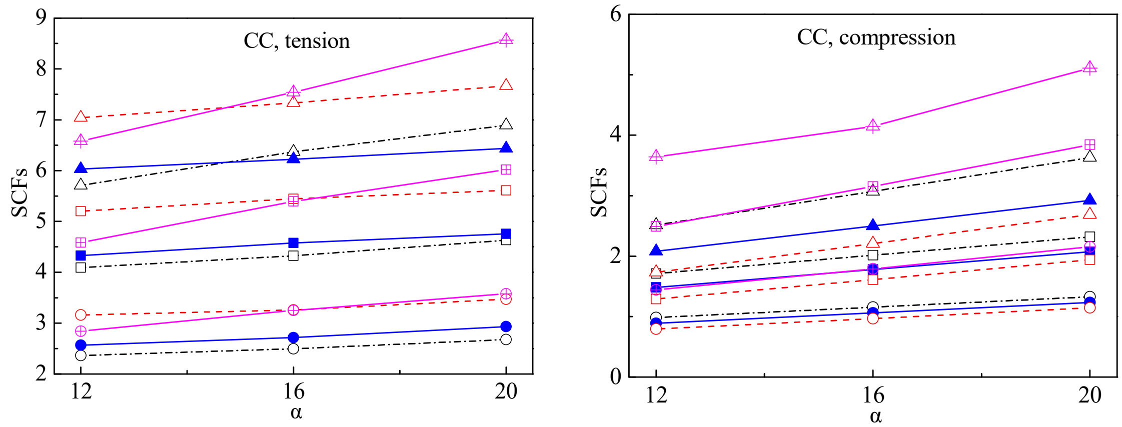

(b) SCF_{CC} vs. α

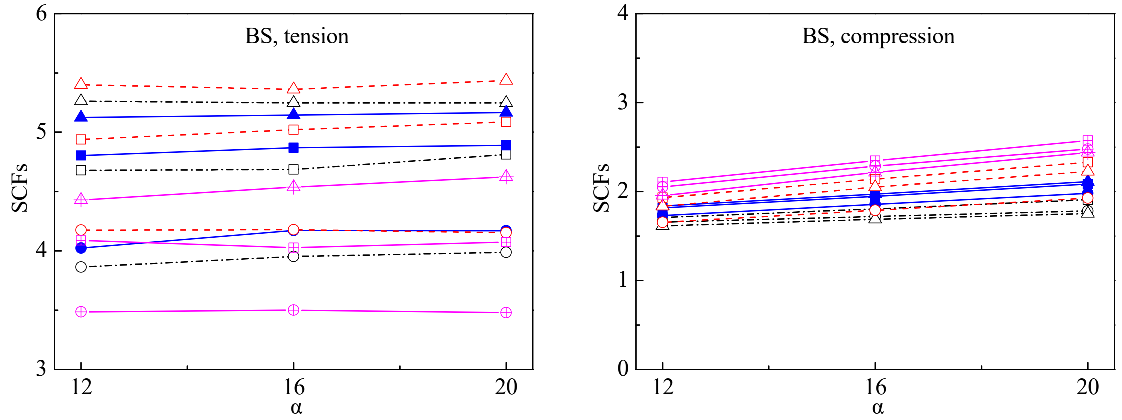

(c) SCF_{BS} vs. α

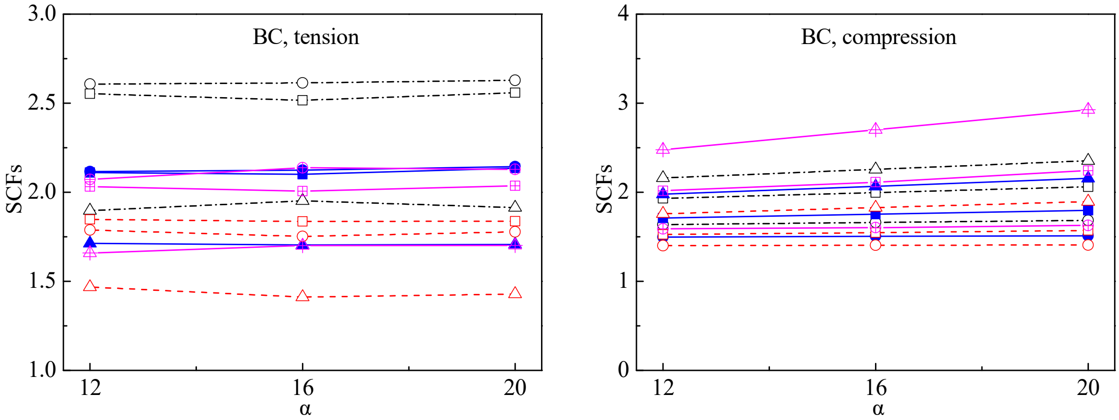

(d) SCF_{BC} vs. α

β=0.3, 2γ=40, τ=0.4
β=0.3, 2γ=40, τ=0.7
β=0.3, 2γ=40, τ=1.0
β=0.4, 2γ=60, τ=0.4
β=0.4, 2γ=60, τ=0.7
β=0.4, 2γ=60, τ=1.0
β=0.5, 2γ=80, τ=0.4
β=0.5, 2γ=80, τ=0.7
β=0.5, 2γ=80, τ=1.0
β=0.6, 2γ=40, τ=0.4
β=0.6, 2γ=40, τ=0.7
β=0.6, 2γ=40, τ=1.0

Fig. 13 Influence of α on SCFs under axial tensile and compressive force in the brace

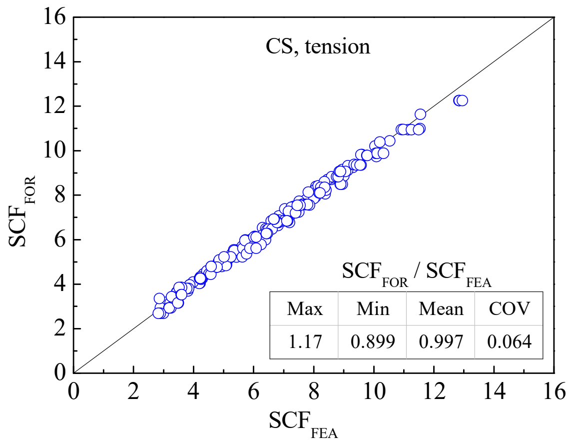

(a) CS: axial tensile fore in brace

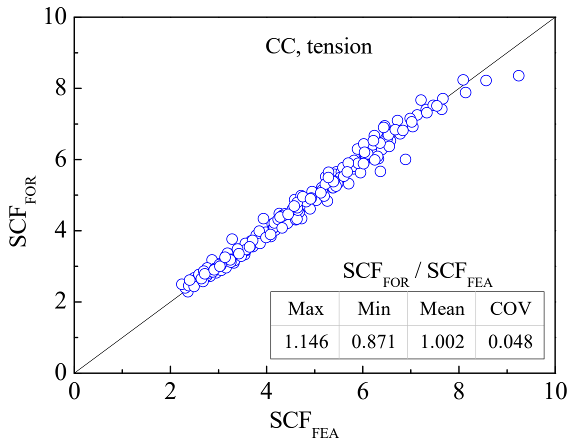

(b) CC: axial tensile fore in brace

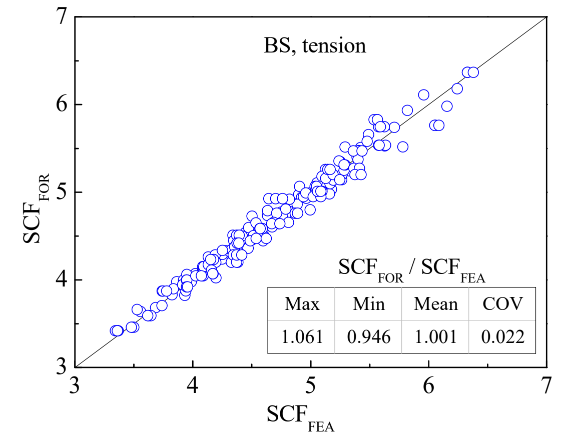

(c) BS: axial tensile fore in brace

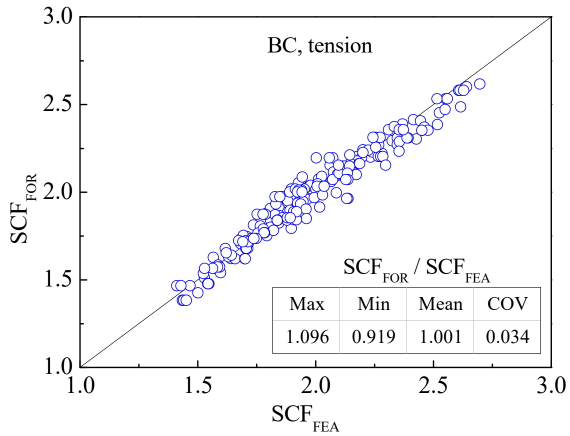

(d) BC: axial tensile fore in brace

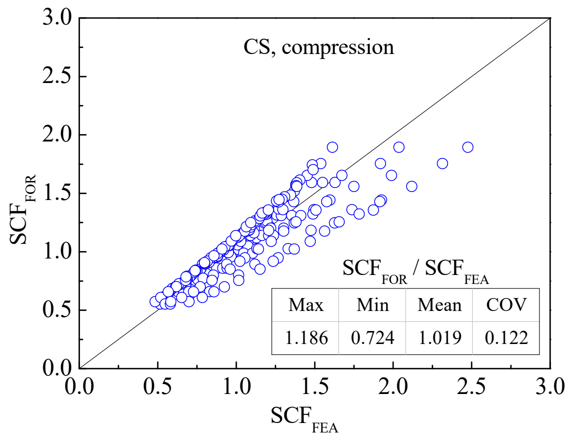

(e) CS: axial compressive fore in brace

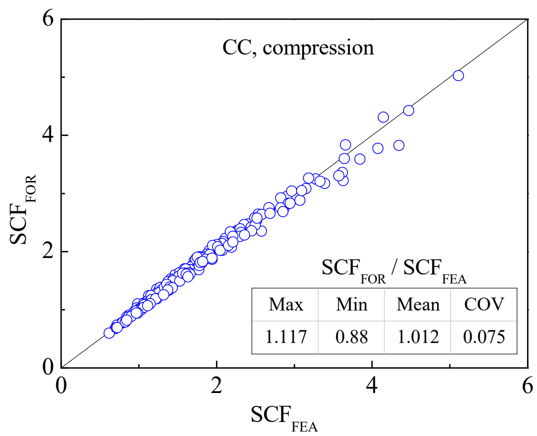

(f) CC: axial compressive fore in brace

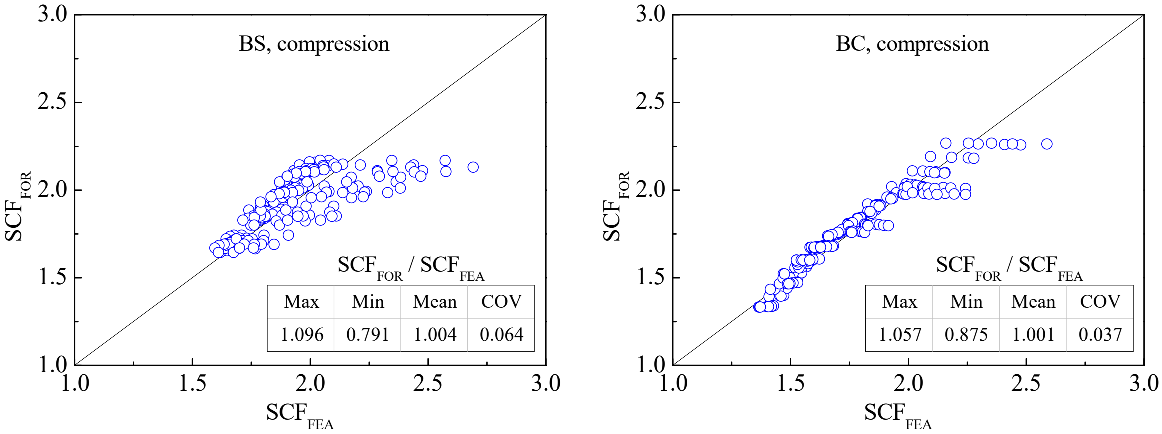

(g) BS: axial compressive fore in brace (h) BC: axial compressive fore in brace

Fig. 14 Comparison of SCF_{FOR} with SCF_{FEA}

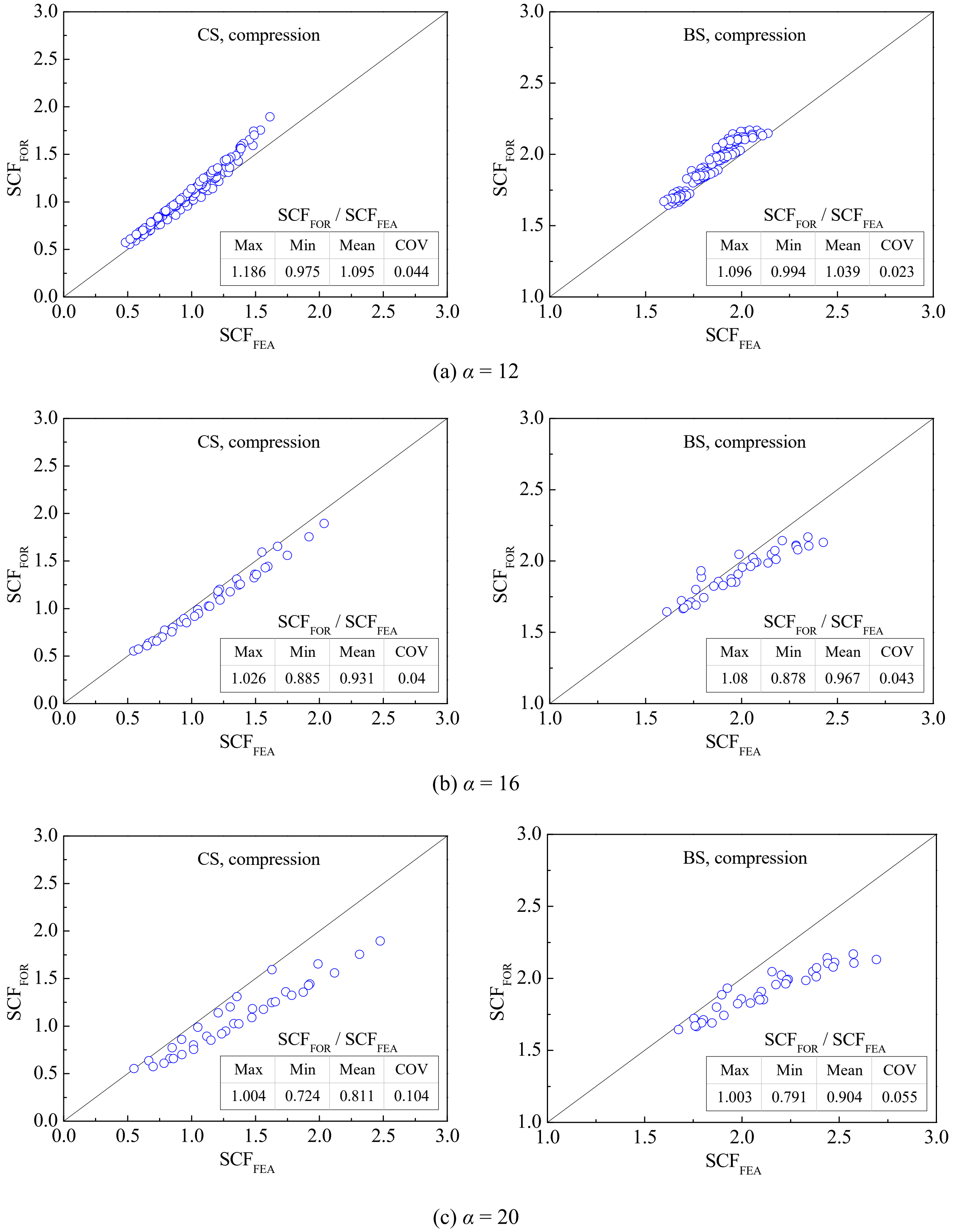

Fig. 15 Comparison of SCF_{FOR} with SCF_{FEA} at locations CS and BS under compression for each α-value